Mechanical Hardness and Adhesion Property of Surface-Polymerized Nanocomposites based on Polyaniline and Sol-Gel Silica

Young Been Lee, Chung Hyoi Park, Sung Kyu Jang and Felix Sunjoo Kim[*]

School of Chemical Engineering and Materials Science, Chung-Ang University, Seoul 06974, Korea

We have investigated the mechanical hardness and adhesion property of electrically conductive polyaniline (PANI) and polyaniline/silane composites prepared on a glass substrate by using a simple polymerization and deposition method. The formation of the conducting nanocomposites was verified by spectroscopic analyses and electron microscopy imaging. The polyaniline films formed in the presence of (3-aminopropyl)triethoxysilane (APTES) were observed to exhibit a remarkable enhancement in their hardness. The nanoindentation study showed that, as the concentration of APTES was increased from 0 to 66.7 wt%, the loading required for a displacement of 25 nm increased from 0.1 to 10.1 μN. Improved adhesion was observed even after 10 peel-off test cycles using commercially available 3M tape. A comparison between the silane materials showed that APTES, owing to the presence of catalytic amine groups, formed more robust composites than tetraethyl orthosilicate (TEOS) under the given processing conditions. The results of our study demonstrate that mechanically rugged polyaniline/silane composite films can be used as pH sensors.

I. INTRODUCTION

Highly conductive polymers, such as polyaniline (PANI), polypyrrole, and polythiophene derivatives, have been extensively studied in the past few decades because of their easy polymerization, low cost, redox properties, wide conductivity range, and ability to be chemically doped with acids [1–14]. The doping/dedoping characteristics of polyaniline have potential applications, *e.g.*, in chemical sensors for acids and bases. Acid doping of polyaniline results in the formation of a conductive emeraldine salt while its dedoping by exposure to a base such as ammonia results in the formation of an insulating emeraldine base [9]. However, despite its promising pH-sensing applications, polyaniline often fails to meet the mechanical robustness required for certain applications. Hence, the easy fabrication and application of polyaniline films on various substrates should be accompanied by chemical/mechanical ruggedness against delamination and scratch.

Delamination and mechanical failure of polymer films under harsh chemical conditions generally deteriorate the performance and the lifetime of devices: therefore, this is a significant problem in sensor applications. Delamination of polymer thin films is commonly a result of mechanical stress (for example, volume change or defor-

mation) and poor adhesion. A polymer film expands due to swelling caused by solvents and/or ions, and contracts when the extrinsic component escapes from the film [15, 16]. Various physical and chemical strategies, such as pretreating the substrate with silane-functionalized polymers [17, 18], geometric optimization [19, 20], and self-assembled monolayers [21], have been proposed as viable solutions for polymer delamination and mechanical failure. These approaches have a long history for several reasons, such as relatively mild reaction conditions, ability to produce multicomponent systems, and enhanced properties and stability [10,11,22–27].

In this work, we adopted the strategy of forming polymer/inorganic hybrid nanocomposites with silane sol-gel precursors to harden the polyaniline films, and we investigated their hardness and adhesion properties on a substrate. Polyaniline was synthesized on a substrate, following the reportedly fast and effective protocol in the presence of hydrolyzed silane agents [3]. The formation of the conductive nanocomposites was verified by using spectroscopic analyses and electron microscopy imaging. We studied two different organosilanes for the fabrication of the nanocomposites and compared their mechanical robustness and adhesion by using the nanoindentation and the tape-peel-off tests, respectively. We then investigated the response of the composites to contact with a basic solution to demonstrate that these films will not be damaged by chemical stimuli.

[*]E-mail: fskim@cau.ac.kr
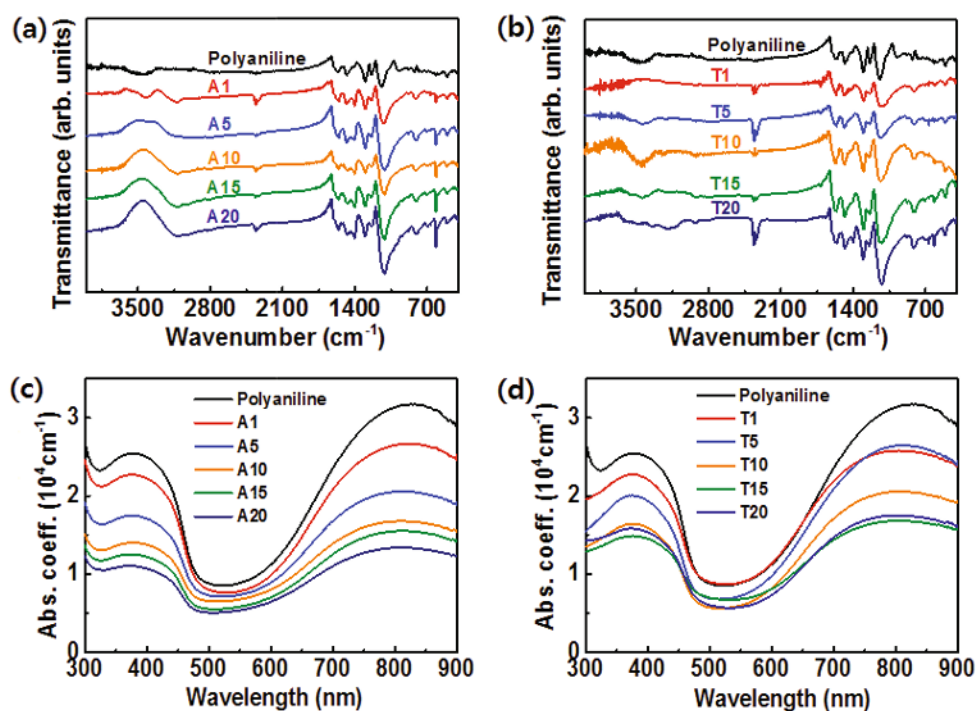
Fig. 1. (Color online) (a), (b) FT-IR and (c), (d) UV/Vis spectra of polyaniline/silane composites: (a), (c) polyaniline/APTES and (b), (d) polyaniline/TEOS.

II. EXPERIMENTS AND DISCUSSION

1. Materials

Aniline, ammonium peroxydisulfate (APS), (3-aminopropyl)triethoxysilane (APTES), and tetraethyl orthosilicate (TEOS) were purchased from Sigma-Aldrich. Hydrochloric acid (HCl) was purchased in the form of an aqueous solution (1 M) from Alfa Aesar. All chemicals were used as received.

2. Fabrication of organosilane/polyaniline films

Aniline and an organosilane precursor, either APTES or TEOS, were first mixed at weight ratios of 10:0, 10:1, 10:5, 10:10, 10:15, and 10:20, and then dissolved in a 1-M HCl solution with 0.6-M aniline. Similarly, 0.6-M APS was dissolved in a separate HCl solution to prepare the initiator solution. A glass substrate was cut (2 cm by 2 cm) and cleaned by using bath sonication with water, acetone, and isopropanol for 15 min each. Solutions of aniline/silane (570 μL) and APS (190 μL) were sequentially dropped at a volume ratio of 3:1 to allow the polymerization for 10 min. The excessive polymers and residual materials were then washed away using acetone. The films were dried in a vacuum oven at room temperature for 24 h. Whenever necessary, a part of the hybrid films was etched using a razor blade, and gold electrodes (50 nm) were deposited onto the films by thermal evaporation.

3. Characterization

Fourier-transform infrared spectroscopy (FT-IR; Perkin-Elmer) was conducted using a KBr pellet. Ultraviolet-visible spectra were recorded using a V-670 spectrophotometer (UV-Vis; JASCO). The morphology of the samples was imaged by using field-emission scanning electron microscopy (FE-SEM; SIGMA, Carl Zeiss). Nano-indentation was performed at room temperature using an ultraprecision surface mechanical analyzer (NANO-IND; Anton Parr) equipped with a Berkovich tip. The peel-off test was performed with a 3M tape. The four-point probe method was used in a glove box filled with nitrogen to measure the resistance of the films. An Agilent 34401A multimeter was used to record the resistance in real time.

III. RESULTS AND DISCUSSION

Our strategy was to polymerize the aniline monomers in the presence of an oxidizer and hydrolyzed silane agents on a substrate. We used the surface polymerization method to demonstrate the coating of an electrically conductive polyaniline film on various substrates and studied the processing-property relationship [3]. For this, we used (3-aminopropyl)triethoxysilane (APTES) and tetraethyl orthosilicate (TEOS), which are the two most widely studied organosilane materials with a structural similarity. APTES contains a primary amine group
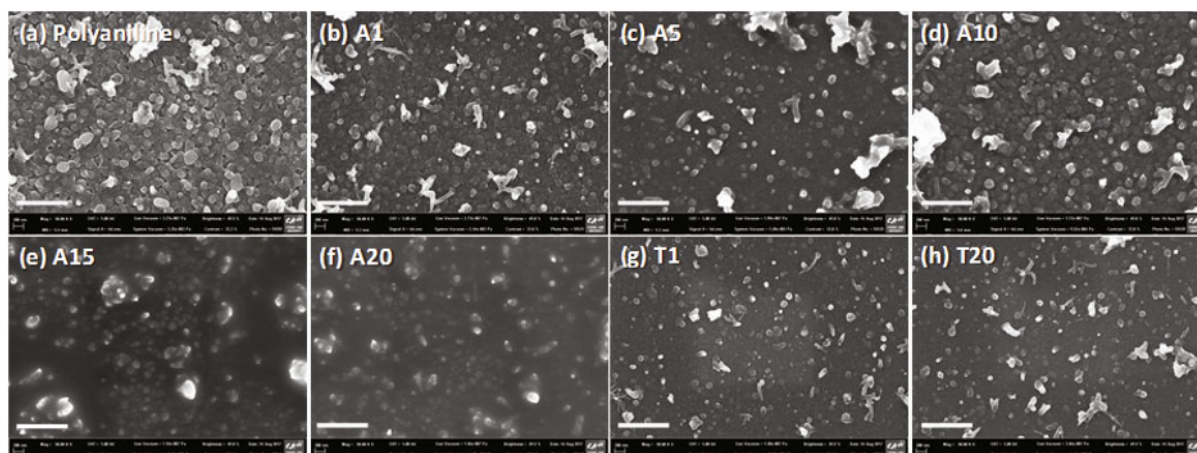
Fig. 2. FE-SEM images of polyaniline/silane hybrid composite films: (a) polyaniline, (b) A1, (c) A5, (d) A10, (e) A15, (f) A20, (g) T1, and (h) T20. The scale bar represents 1 μm.

that can also function as a catalyst during silane coupling. As the organosilane is premixed with aniline in an aqueous acidic solution, it undergoes partial hydrolysis and condensation, forming small and irregular particles. Herein, we used Ax and Tx, respectively, to represent the polyaniline/APTES and the polyaniline/TEOS samples for an aniline:silane weight ratio of 10:x.

The successful formation of the hybrid composites was observed by using FT-IR and UV/Vis spectroscopic analyses (Fig. 1). The IR peaks for polyaniline at 1148 cm^{-1} and 1304 cm^{-1} correspond to the aromatic in-plane C-H bending peak and C-N bonding of the secondary aromatic amine, respectively. The peaks around 1482 cm^{-1} and 1581 cm^{-1} are, respectively, attributed to the stretching of the benzenoid and quinoid rings of polyaniline [28]. Thus, polyaniline is evidently well polymerized in the presence of APTES or TEOS. As the hydrolysis and condensation reactions for silane progress, the siloxane peaks are observed to evolve at 1000–1260 cm^{-1} from the asymmetric stretching peak of the Si-O-Si bond [29]. The broad peak at 3200 cm^{-1} can be attributed to the CH$_2$-NH$_2$ bond [30]. The peaks at 800 cm^{-1} and 615 cm^{-1} correspond to the symmetric Si-O-Si stretching of the four-fold siloxane ring [31]. The peak intensities at 3200 cm^{-1} and 615 cm^{-1} are observed to gradually increase with increasing APTES concentration, supporting the formation of Si-O-Si linkages in the films. On the other hand, relatively smaller changes are observed in the IR spectra of the TEOS samples compared with those of the APTES samples: the peaks were slightly increased only for T20, which is the sample with the highest TEOS concentration. The difference in the spectra between these two composite systems may be attributed to the condensation rate, which depends on the pH and the processing conditions: The condensation in TEOS is not significant at low pH values, which is around 2 [32]. On the other hand, the presence of the amine group in APTES causes the aniline/APTES solution to be rela-

tively basic, enabling effective condensation reactions.

The UV-vis spectra provide information on the doping state of polyaniline and the compositions of the composite films. The polyaniline in the composites is in the emeraldine salt phase, as evidenced by the bands around 350 nm, which is attributed to the π-π^* transition of benzenoid, and the peaks at 400–412 nm and 800–830 nm indicate the occurrence of polaronic transitions (Figs. 1(c) and (d)) [33,34]. This observation suggests that the doped state of polyaniline is not affected by the presence of silane components. Unlike the doping state, the absorption coefficient was affected by the concentration of silane. Because silica functions as a translucent matrix, the intensity of the UV-vis absorption, as expected, decreases with increasing silane content in the composite.

Figure 2 shows the FE-SEM images of the polyaniline composite films. The pristine polyaniline film without silane is observed to have typical granular or short rod-like structures of polymers that are fused with each other. The diameter of the polyaniline particulates is approximately 200–300 nm, and the granular shape is consistent in the composite films. However, addition of APTES or TEOS results in a morphological variation. The gaps between the polyaniline particulates in the composites are filled with inorganic components. Thus, the granular structures are embedded in a uniform, dense, and nonconducting siloxane matrix as the concentration of silane is increased. This dense structure is believed to be beneficial for the mechanical ruggedness of the composites.

Figure 3 shows the electrical properties of the composite films as a function of the silane concentration. In the APTES composites, the thickness progressively increases from 338 to 831 nm when the APTES concentration is increased from 0 to 66.7 wt%, with a marginal decrease in the resistance, i.e., from 506 to 466 Ω. As a result, the electrical conductivity monotonically decreases from 12.9 to 5.7 S/cm. Considering the APTES concentra-
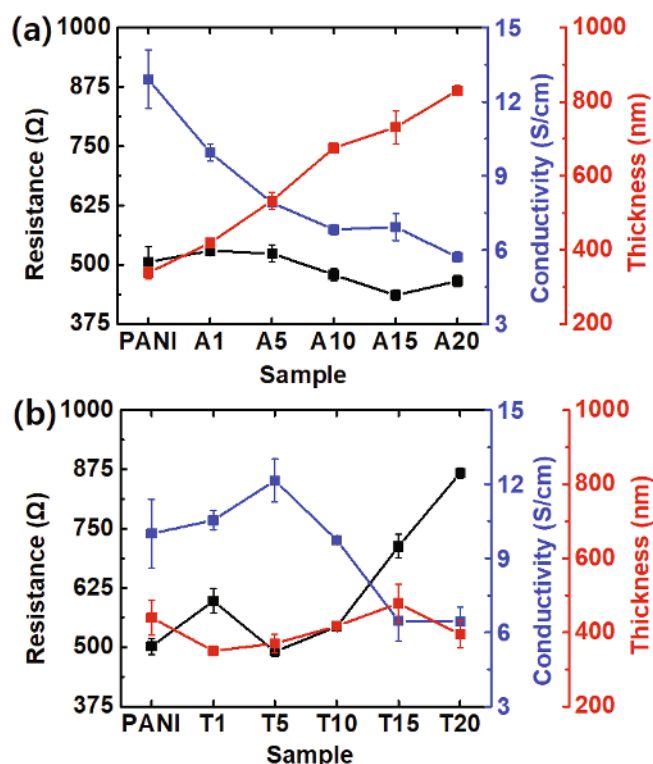
Fig. 3. (Color online) Resistance, thickness, and electrical conductivity of polyaniline/silane composite films: (a) APTES and (b) TEOS.

Fig. 4. (Color online) Nanoindentation curves for the polyaniline/silane composite films.

tion, the charge-transport ability of the composite is well maintained, and a low percolation threshold can be expected. However, the thickness (*i.e.*, 400–500 nm) of the composite samples increases only slightly with increasing TEOS concentration, while the increase in the resistance of the polyaniline/TEOS composites is quite significant (*i.e.*, from 500 to 868 Ω); this results in a decrease in the conductivity to 6.4 S/cm in T20.

The mechanical hardness of the samples was characterized by using the nanoindentation test. Figure 4 shows that the reference polyaniline requires a very small load (0.1 μN) for a displacement of 25 nm. Similarly, the samples A1, A5, and A10 also exhibit significant displacements with small loads ($\leq$0.6 μN). The load required for a 25-nm displacement is observed to sharply increase to 3.5 and 10.1 μN for A15 and A20, respectively. Furthermore, the indentation force of A15 is almost 10 times higher than that of A10, clearly demonstrating its good mechanical property. This sharp increase in the indentation force can be translated into an increased hardness of the composite films, confirming the considerable effect of APTES concentration on hardness. This is because of the high solidity induced by the considerable number of cross-linked siloxane groups and inorganic particles, which effectively function as a matrix for the polyaniline films. Likewise, the T20 sample exhibits an indentation loading of 3.2 μN for a 25-nm displacement, which is

close to that of A15 and one-third that of A20. This difference suggests that, under the given processing conditions, the cross-links in APTES are more effective and form a harder matrix than those in TEOS do.

In addition to hardness, the adhesion between the films and the glass substrate was also observed to be enhanced. To investigate this adhesion property, we performed the tape-peel-off test (Fig. 5). We observed a 14.7% increase in the resistance of the polyaniline composites with 66.7 wt% APTES (A20) after 10 test cycles, whereas the pure polyaniline films were detached from the substrate as early as in the third cycle. We also observed that even a small amount of APTES (9 wt%) could effectively enhance the adhesion and maintain the electrical pathway in the composite films; this is because we could track the resistance changes even for the A1 sample. Moreover, although conjugated polymer films such as polyaniline have a relatively low adhesion and mechanical integrity with increasing thickness, the adhesion of the polyaniline/APTES composites was observed to be superior even at a thickness of 831 nm. The matrix formed by the APTES particulates not only contributes to the hardness enhancement, but also participates in the adhesion with the glass substrate through siloxane bonding, thereby enhancing the mechanical integrity of the composites. Similarly, compared with pristine polyaniline, adhesion was also enhanced in the sample with TEOS. However, the polyaniline/TEOS composites exhibited a monotonic increase in the resistance: the change in resistance was much larger (>100%) in the TEOS composites than in the APTES composites, again suggesting that APTES is more effective in enhancing the mechanical robustness.

We next measured the resistance change of these rugged composites on exposure to ammonium hydroxide (Fig. 6). Pristine polyaniline gets dedoped, changes color from green to blue, and becomes less conductive, when
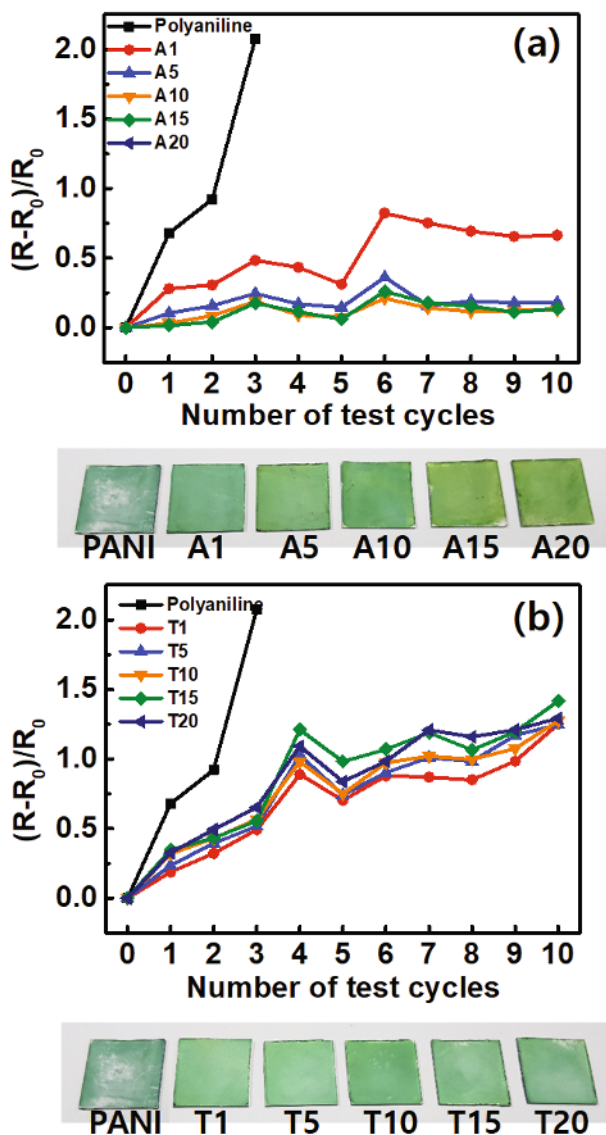
Fig. 5. (Color online) Resistance change in the polyaniline/silane composites with (a) APTES and (b)TEOS during the tape-peel-off test, along with photographs of the composites after 10 cycles.

the film contacts a basic solution. The pristine polyaniline also gets damaged when a drop of a basic solution is placed on the film. The polyaniline/APTES composites, however, can withstand the harsh conditions. As a result, the detection of a basic solution is more stable with the composites, enabling their use as simple pH sensors. When detecting the presence of ammonium hydroxide, the relative changes in resistance were observed to be the largest in the A1 sample, while the degree of response was observed to be weaker for the composite films with a higher silane concentration. This is due to the dense siloxane matrix of the composites, which prevents easy penetration of ions into the films.
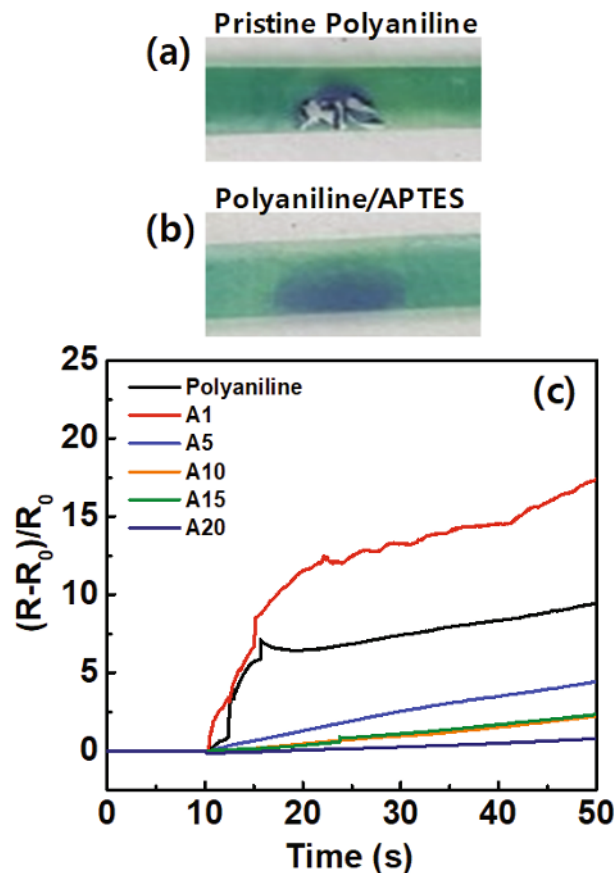
Fig. 6. (Color online) Response of polyaniline/silane composites to ammonium hydroxide. (a) Damage and dedoping of pristine polyaniline. (b) Dedoping of the polyaniline/APTES composite. (c) Resistance change of polyaniline/silane films when exposed to ammonium hydroxide solution (0.01 M).

IV. CONCLUSION

We demonstrated that mechanically robust and electrically conductive polyaniline composites with enhanced adhesion can be deposited on a glass substrate by using a simple polymerization and deposition method. Spectroscopic analyses such as UV-vis and FT-IR revealed the successful formation of the composites while the electron microscope imaging showed polyaniline particulates embedded in the silica matrix. As expected from the insulating silica, the electrical conductivity slightly decreased with the addition of silane to the composites. The nanoindentation and the tape-peel-off tests revealed enhanced hardness and adhesion through composite formation. A comparison between the silane materials showed that APTES forms more robust composites than TEOS under the given processing conditions. Thus, the improved mechanical properties of the films endow the use of the polyaniline/silane composites as a rugged pH sensing platform in a liquid flow environment.

ACKNOWLEDGMENTS

REFERENCES

[1] Y. Xia, A. G. MacDiarmid and A. J. Epstein, Macromolecules **27**, 7212 (1994).

[2] A. G. MacDiarmid, Synth. Met. **84**, 27 (1997).

[3] C. H. Park, S. K. Jang and F. S. Kim, Appl. Surf. Sci. **429**, 121 (2018).

[4] S. K. Jang, J. Choi and F. S. Kim, J. Nanosci. Nanotechnol. **17**, 7793 (2017).

[5] A. C. B. Tavares, I. A. Hümmelgen and M. S. Meruvia, Org. Electron. **54**, 114 (2018).

[6] X. Wei, H. Zou and S. Gao, Carbon **123**, 471 (2017).

[7] U. Male and B. K. Shin, Macromol. Res. **25**, 1121 (2017).

[8] N. R. Chiou and A. J. Epstein, Adv. Mater. **17**, 1679 (2005).

[9] S. Virji, J. Huang, R. B. Kaner and B. H. Weiller, Nano Lett. **4**, 491 (2004).

[10] Q. Wang *et al.*, Macromolecules **36**, 5760 (2003).

[11] M. Ita, Y. Uchida and K. Matsui, J. Sol-Gel Sci. Technol. **26**, 479 (2003).

[12] L. Li, Y. Guo, C. Zhao and L. Song, Macromol. Res. **26**, 592 (2018).

[13] S. W. Kang and J. Bae, Macromol. Res. **26**, 226 (2018).

[14] J. Choi, S. K. Jang and F. S. Kim, Phys. Status Solidi A **215**, 1701019 (2018).

[15] E. Smela, O. Inganas and I. Lundstrom, Science **268**, 1735 (1995).

[16] M. R. Abidian, J. M. Corey, D. R. Kipke and D. C. Martin, Small **6**, 421 (2010).

[17] L. Cecchetto, A. Denoyelle, D. Delabouglise and J.-P. Petit, Appl. Surf. Sci. **254**, 1736 (2008).

[18] C. Zhang, N. E. Shephard, S. M. Rhodes and Z. Chen, Langmuir **28**, 6052 (2012).

[19] C. Yu *et al.*, ACS Appl. Mater. Interfaces **6**, 8199 (2014).

[20] A. J. Crosby, M. Hageman and A. Duncan, Langmuir **21**, 11738 (2005).

[21] L. F. Rozsnyai and M. S. Wrighton, Chem. Mater. **8**, 309 (1996).

[22] R. Roy, Science **238**, 1664 (1987).

[23] U. Schubert, N. Huesing and A. Lorenz, Chem. Mater. **7**, 2010 (1995).

[24] C. J. Brinker and G. W. Scherer, *Sol-Gel Science: The Physics and Chemistry of Sol-Gel Processing* (Academic press, 2013).

[25] N. J. Terrill, T. Crowley, M. Gill and S. P. Armes, Langmuir **9**, 2093 (1993).

[26] H. Xia and Q. Wang, J. Appl. Polym. Sci. **87**, 1811 (2003).

[27] P. Liu, Curr. Opin. Solid State and Mater. Sci. **12**, 9 (2008).

[28] J. Tang, X. Jing, B. Wang and F. Wang, Synth. Met. **24**, 231 (1988).

[29] R. M. Pasternack, S. R. Amy and Y. J. Chabal, Langmuir **24**, 12963 (2008).

[30] M. Gueye *et al.*, Plasma Process. Polym. **13**, 698 (2016).

[31] H. Yoshino, K. Kamiya and H. Nasu, J. Non-Cryst. Solids **126**, 68 (1990).

[32] D. Li *et al.*, J. Mater. Chem. **22**, 15702 (2012).

[33] J. E. Albuquerque *et al.*, Synth. Met. **113**, 19 (2000).

[34] S. Bai *et al.*, Small **11**, 306 (2015).